A Blind Synchronizer for OFDM Systems Based on SINR Maximization in Multipath Fading Channels

Wen-Long Chin and Sau-Gee Chen

***Abstract*—This paper presents a blind synchronizer for orthogonal frequency-division multiplexing (OFDM) systems based on signal-to-interference-and-noise ratio (SINR) maximization. Due to the incurred losses from intersymbol interference (ISI) and intercarrier interference (ICI) introduced by synchronization errors, the SINR of the received data drastically drops. By taking advantage of this characteristic, both the symbol time and carrier frequency offsets are intuitively estimated by maximizing the SINR metric. For the SINR metric, two blind SINR estimations are investigated. The estimations do not need prior knowledge of the channel profiles and transmitted data. As such, the proposed maximum SINR (MSINR) synchronization algorithm is nondata aided so that the transmission efficiency can be improved. Moreover, to reduce the computational complexity, the early–late gate technique is proposed for the implementation of the synchronizer. Simulation results exhibit better performance for the MSINR algorithm than conventional techniques in multipath fading channels.**

***Index Terms*—Blind synchronization, early–late gate (ELG), orthogonal frequency-division multiplexing (OFDM), signal-to-interference-and-noise-ratio (SINR) maximization.**

I. Introduction

ORTHOGONAL frequency-division multiplexing (OFDM) is a promising technology for broadband transmission due to its high-spectrum efficiency and its robustness to the effects of multipath fading channels and impulse noises [1]–[4]. OFDM has been adopted by many state-of-the-art communication standards such as digital video broadcasting–terrestrial, digital audio broadcasting, digital subscriber line, wireless local area network systems based on 802.11x standards, and fixed or mobile ad hoc network systems based on 802.16x standards. It has also become a key technology in mobile communication systems beyond third generation.

However, OFDM systems are sensitive to synchronization errors. First, uncertain OFDM symbol arrival time introduces a symbol time offset (STO), and the coarse symbol time (CST) [5] and fine symbol time (FST) [6], [7] estimations are needed. Second, the mismatch of the oscillators in carrier frequencies (CFs) between the transmitter and the receiver produces a CF offset (CFO) so that the resulting fractional CFO (FCFO) [5], integral CFO (ICFO) [8], and residual CFO (RCFO) [6], [7] have to be eliminated. Moreover, the mismatch of sampling clocks between the digital-to-analog converter and the analog-to-digital converter introduces a sampling CFO (SCFO) [7].

The symbol time (ST) estimation is usually the first step in an entire OFDM synchronization process, because it provides an estimated symbol boundary for the remaining synchronization steps. When the ST is located in the intersymbol interference (ISI)-free region, no ISI results, and only phase rotation in the demodulated frequency-domain data occurs, which can simply be compensated by using the single-tap equalizer. If channels are time variant, aside from ISI, extra channel-induced intercarrier interference (ICI) is inevitable. The CFO and SCFO introduce additional ICI.

In [5], the STO and the FCFO are jointly estimated by a delayed-correlation algorithm. It is a maximum-likelihood (ML) estimation and is only good for the additive white Gaussian noise (AWGN) channels. In [9], a new method that uses training symbols in time domain was proposed. However, its correlation result exhibits an uncertain plateau in multipath fading channels [10]. A remedy for this ambiguity is proposed in [10]. Some techniques [6], [9]–[12] have good ST performances. However, extra time-domain training symbols are needed. Although the technique in [13] can identify the ISI-free region in multipath fading channels, for an accurate ST estimation, it may involve many symbols. In [6] and [7], the channel frequency response (CFR) must first be estimated. The inverse fast Fourier transform (IFFT) is then applied to obtain the channel impulse response (CIR), which is then used to adjust the symbol boundary. The work in [14] treats the CST estimation in multipath fading channels. Some works locate the symbol boundary at the sampling instance that has the minimum interference [15]–[17] or maximum correlation result of the cyclic prefix (CP) [5]. The interference is used as the metric in the minimum-interference ST estimators.

The proposed scheme aims to effectively reduce the synchronization errors, including the STO and the CFO, so that the signal-to-interference-and-noise-ratio (SINR) is maximized. In other words, we consider not only the interference power but also the signal power. We investigate two blind SINR estimations (without needing prior knowledge of the channel profiles and transmitted data) for the proposed maximum-SINR (MSINR) synchronization algorithm. The MSINR algorithm is nondata aided (NDA) so that the bandwidth efficiency can be improved. In addition, to reduce the computational complexity, an early–late gate (ELG) technique is also proposed for the implementation of the new MSINR algorithm.

Manuscript received September 17, 2007; revised March 6, 2008, May 3, 2008, and May 4, 2008. First published May 14, 2008; current version published February 17, 2009. This work was supported in part by Grant NSC 95-2219-E-009-004 and Grant MOEA 95-EC-17-A-01-S1-048, Taiwan. The review of this paper was coordinated by Dr. K. T. Wong.

W.-L. Chin is with the Department of Engineering Science, National Cheng Kung University, Tainan 701, Taiwan (e-mail: johnsonchin@pchome.com.tw).

S.-G. Chen is with the Department of Electronics Engineering and Institute of Electronics, National Chiao Tung University, Hsinchu 30050, Taiwan.

Digital Object Identifier 10.1109/TVT.2008.925320

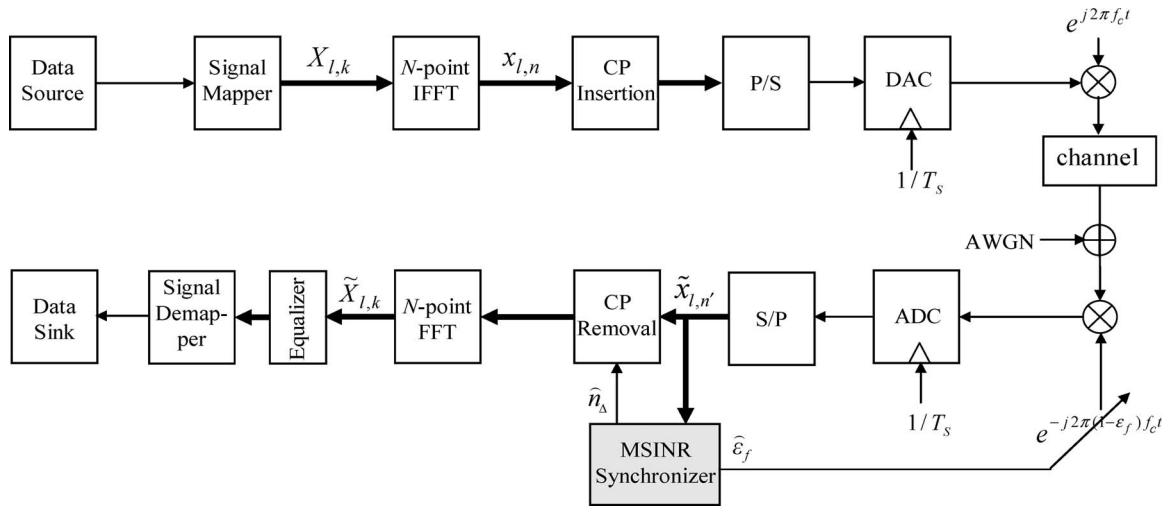

Fig. 1. Simplified OFDM system model. The MSINR synchronizer operates in the frequency domain by utilizing the FFT operations. A detailed block diagram of the synchronizer can be found in Fig. 7.

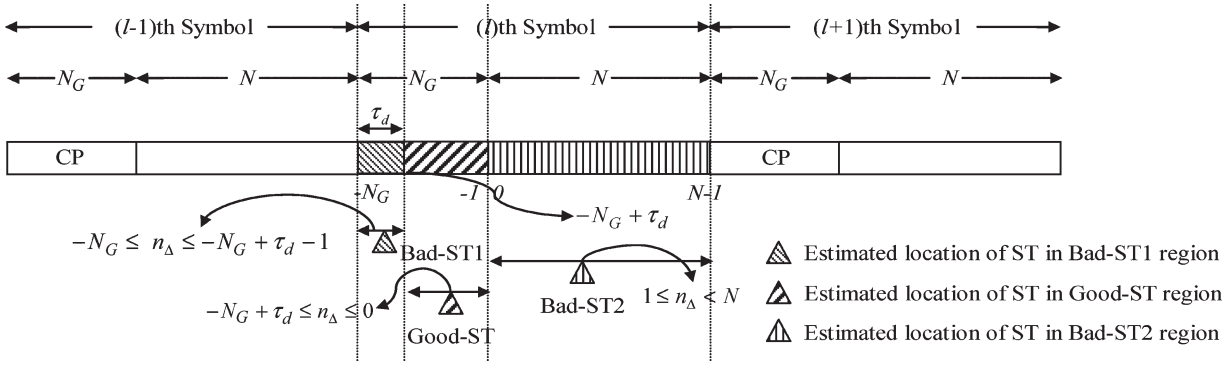

Fig. 2. Three different ST regions.

The rest of this paper is organized as follows. The OFDM system and signal models in multipath fading (slow-fading, block-fading, flat fading) channels are introduced in Section II. The MSINR synchronization algorithm and the ELG technique are detailed and analyzed in Section III. The performance is analyzed in Section IV. Simulation results are provided in Section V. Finally, we conclude our paper in Section VI.

II. OFDM System and Signal Models

In the following discussion, all the quantities indexed with l belong to the lth symbol. A simplified OFDM system model is shown in Fig. 1, where $X_{l,k}/\tilde{X}_{l,k}$ is the transmitted/received frequency-domain data at the kth subcarrier, $x_{l,n}$ is the transmitted time-domain data after the IFFT, and $\tilde{x}_{l,n'}$ is the received time-domain data, where $-N_G n' < N$, N is the number of subcarriers, and N_G is the CP length. $1/T_S$ is the sampling frequency, ε_f is the CFO (normalized by the subcarrier spacing), f_c is the CF, $\widehat{n}_\Delta$ is the estimated STO, and $\widehat{\varepsilon}_f$ is the estimated CFO. On the transmitter side, N complex data symbols are modulated onto N subcarriers by using the IFFT. The last N_G IFFT output samples are copied to form the CP that is inserted at the beginning of each OFDM symbol. By inserting the CP, a guard interval is created so that ISI can be avoided and the orthogonality among subcarriers can be sustained. The receiver uses the fast Fourier transform (FFT) to demodulate received data.

As shown in Fig. 2, an estimated ST generally falls into one of the three regions of an OFDM symbol: 1) the Bad-ST1 region, 2) the Good-ST region (also known as the ISI-free region), and 3) the Bad-ST2 region in which the STO n_Δ is confined within the ranges of $-N_G \le n_\Delta \le -N_G + \tau_d - 1$, $-N_G + \tau_d \le n_\Delta \le 0$, and $1 \le n_\Delta \le N - 1$, respectively, where τ_d is the maximum delay spread of the channel. The Bad-ST1 and Good-ST regions are in the guard interval of length N_G. When the ST is located in the Good-ST region, no ISI results; however, when the ST is located in the Bad-ST1 and Bad-ST2 regions, the lth symbol has ISI from the $(l-1)$th and $(l+1)$th symbols, respectively. There is freedom to select the ST in the Good-ST region. This region is obviously defined by the channel length. Hence, for good ST estimation, one should consider the channel effect to avoid the ISI such that the SINR is maximized. The STO is with reference to the ideal ST of the lth symbol, which is marked by the time index at zero. Detailed analysis of the received frequency-domain data (at the kth subcarrier) in these three regions can be found in [18], and the results are rewritten as follows (for only the Bad-ST2 region):

$$\tilde{X}_{l,k} = \tilde{X}^d_{l,k} + \tilde{N}_k \tag{1}$$

where

$$\tilde{X}^d_{l,\,k} \triangleq \frac{N-n_\Delta}{N} H_k X_{l,\,k} W_N^{(-lN_s\varepsilon_f - kn_\Delta)} \tag{2}$$

is the desired data, H_k is the CFR at the kth subcarrier, W_N is $e^{-j2\pi/N}$, and $N_S = N + N_G$ is the OFDM symbol length, including the CP. In addition

$$\tilde{N}_k \triangleq \frac{1}{N}\sum_{m\neq k}\sum_{n'=0}^{N-1} W_N^{-n'(m-k+\varepsilon_f)} H_m X_{l,m} \times W_N^{(-lN_s\varepsilon_f - kn_\Delta)} + v_k - \tilde{X}^{\text{ici}}_{l,\,k} + \tilde{X}^{\text{isi}}_{l,\,k} \tag{3}$$

is the combined interference and the AWGN v_k, where

$$\tilde{X}^{\text{ici}}_{l,\,k} = \frac{1}{N}\sum_{m\neq k}\sum_{n'=N-n_\Delta}^{N-1} W_N^{-n'(m-k+\varepsilon_f)} \times H_m X_{l,m} W_N^{(-lN_s\varepsilon_f - kn_\Delta)} \tag{4}$$

is the ICI term, and

$$\tilde{X}^{\text{isi}}_{l,\,k} = \frac{1}{N}\sum_{m}\sum_{n'=N-n_\Delta}^{N-1} W_N^{-n'(m-k+\varepsilon_f)} H_m X_{l+1,m} \times W_N^{(-lN_s\varepsilon_f - k(n_\Delta+N_G))} \tag{5}$$

is the ISI term. Note that the dependence of the received frequency-domain data on the STO and CFO is dropped for notational clarity. It can easily be shown that the desired signal power is

$$\sigma^2_{\tilde{X}^d_{l,\,k}} = E\left[\left|\tilde{X}^d_{l,\,k}\right|^2\right] = \left(\frac{N-n_\Delta}{N}\right)^2 m_{|X|^2}|H_k|^2 \tag{6}$$

and the combined interference and AWGN power is

$$\begin{aligned}\sigma^2_{\tilde{N}_k} &= E\left[|\tilde{N}_k|^2\right] \\ &= \frac{m_{|X|^2}}{N^2}\left\{\sum_{m\neq k}\sum_{n_1=0}^{N-1}\sum_{n_2=0}^{N-1} W_N^{-(n_1-n_2)(m-k+\varepsilon_f)}|H_m|^2 \right. \\ &\quad + \sum_{n_1=N-n_\Delta}^{N-1}\sum_{n_2=N-n_\Delta}^{N-1} W_N^{-(n_1-n_2)\varepsilon_f}|H_k|^2 \\ &\quad + 2\sum_{m\neq k}\sum_{n_1=N-n_\Delta}^{N-1}\sum_{n_2=N-n_\Delta}^{N-1} \\ &\quad \left. \times W_N^{-(n_1-n_2)(m-k+\varepsilon_f)}|H_m|^2 + \sigma^2_{v_k}\right\}\end{aligned} \tag{7}$$

where $m_{|X|^2} = E[|X_{l,\,k}|^2] = E[|X_{l+1,\,k}|^2]$ is the transmitted data power, and $\sigma^2_{v_k}$ is the AWGN power. Finally, the theoretical SINR can be written as

$$\eta_{\text{th}}(n_\Delta, \varepsilon_f) = \frac{\frac{1}{N}\sum_k \sigma^2_{\tilde{X}^d_{l,\,k}}}{\frac{1}{N}\sum_k \sigma^2_{\tilde{N}_k}} \tag{8}$$

which is highly dependent on the STO and CFO.

III. Proposed MSINR Synchronization Technique

When the STO or CFO increases, the signal power decreases, whereas the interference power increases [19], [20], as also suggested in (6) and (7), respectively. Consequently, it is evident that the SINR is a good metric for indicating the synchronization offsets. On the other hand, minimum-interference synchronizers [15]–[17] only consider the interference power. As such, they may have performance losses, because they do not simultaneously consider both the signal and interference power.

A. Blind SINR Estimations for the MSINR Synchronization Algorithm

Before introducing the MSINR synchronization technique, the SINR estimation for (8) is first investigated. It can be realized that a good SINR estimation for an effective synchronizer in practical environments should have the following properties: 1) The estimated SINR profile is a unimodal function of the STO and CFO and has a maximum value at the ideal synchronization point, and 2) the variance of the estimation is small. In the following discussion, we will investigate two blind SINR estimations based on the second and fourth moments of the envelope and evaluate their conformity with these two properties.

1) Time-Oriented SINR Estimation: After an extensive survey of the SINR estimation techniques, we found that in [21], the SINR estimation of a real-valued single-carrier signal is useful due to its simplicity and robustness. It was derived by utilizing the second and fourth moments of the envelope in slow-fading channels. We generalize and extend it to the complex-valued signals for the OFDM systems. It is omitted in this paper because the derivation is similar to [21]. The key parameters and results are written as follows. First, one can define the following second and fourth moments of $|\tilde{X}_{l,\,k}|$ at the kth subcarrier based on time sample averages:

$$M_k \triangleq \frac{1}{L}\sum_l |\tilde{X}_{l,\,k}|^2 \tag{9}$$

$$Q_k \triangleq \frac{1}{L}\sum_l |\tilde{X}_{l,\,k}|^4 \tag{10}$$

$$R_k \triangleq \frac{1}{L}\sum_l |\tilde{X}_{l,\,k}|^2 |\tilde{X}_{l+1,\,k}|^2 \tag{11}$$

where L is the number of OFDM symbols. Then, the signal power S_k and interference power I_k at the kth subcarrier can be determined as

$$S_k = \left(M_k^2 + R_k - Q_k\right)^{1/2} \tag{12}$$

$$I_k = M_k - S_k \tag{13}$$

respectively. Finally, the SINR can be obtained by averaging over all subcarriers (in the frequency domain)

$$\widehat{\eta}\,(n_\Delta, \varepsilon_f) = \frac{\frac{1}{N}\sum_k S_k}{\frac{1}{N}\sum_k I_k}. \tag{14}$$

2) Frequency-Oriented SINR Estimation: In the time-oriented method, a slow-fading channel condition is assumed. The channels are possibly fast fading; thus, it is inadequate to average over symbols in (9)–(11). To reflect dynamical environments and derive the SINR profile with enough data samples in a few symbols, we propose to average over all N subcarriers in the frequency domain first. Moreover, under the condition that only one OFDM symbol is available (i.e., $L = 1$), it can be shown that $M_k^2 = Q_k$. Therefore, the signal power S_l' and interference power I_l' can be written as

$$S_l' = \frac{1}{N}\sum_k \left|\tilde{X}_{l,k}\tilde{X}_{l+1,k}^*\right| \tag{15}$$

$$I_l' = \sqrt{\left(\frac{1}{N}\sum_k |\tilde{X}_{l,k}|^2\right)\left(\frac{1}{N}\sum_k |\tilde{X}_{l+1,k}|^2\right)} - S_l' \tag{16}$$

respectively. Note that the geometric average of the total power of two symbols is used to represent the total power. The SINR estimate η_l' of the lth symbol can be written as

$$\eta_l' = S_l'/I_l'. \tag{17}$$

Moreover, the estimation (17) can be averaged over symbols to improve the accuracy.

3) Comparison of the SINR Estimations: The time-oriented (14) and frequency-oriented (17) SINR estimations under various signal-to-noise ratios (SNRs) are qualitatively compared (using the estimated SINR profile) as follows and will quantitatively be compared (using the estimations' variances) in Section V-A.

We assume an OFDM system with the following specifications: $N = 256$, $N_G = 32$, $f_c = 2.4$ GHz, $T_s = 115.2$ μs, and the signal bandwidth is 2.5 MHz. The time-oriented and frequency-oriented SINR estimations against the STO in a time-invariant channel are demonstrated in Fig. 3(a) and (b). The channel is assumed to have N_G paths. Therefore, the Good-ST region contains only one sample (i.e., the zeroth sample in Fig. 2). The channel taps are randomly generated by independent zero-mean, unit-variance complex Gaussian variables. As shown in the figure, both estimated SINR profiles are unimodal and have their maximum values in the Good-ST region (at the zeroth sample). The estimated SINR profiles in a time-variant channel are shown in Fig. 4. The normalized Doppler frequency (NDF) is 0.035. As shown in Fig. 4 and depicted in [21], the time-oriented estimation is more sensitive to the NDF than the frequency-oriented estimation.

The time-oriented and frequency-oriented SINR estimations against the CFO in a time-invariant channel are demonstrated in Fig. 5(a) and (b), where both estimated SINR profiles are unimodal and have their maximum values at CFO $= 0$. The estimated SINR profiles in a time-variant channel are demonstrated in Fig. 6. The NDF is 0.035, and the time-oriented estimation is similarly more sensitive to the NDF than the frequency-oriented estimation.

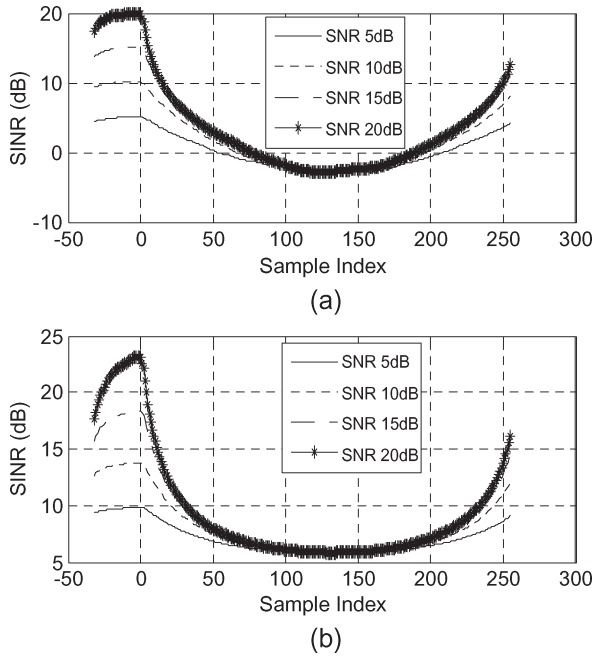

Fig. 3. SINR estimations (14) and (17) against the STO in a time-invariant channel are shown in (a) and (b), respectively. CFO $= 0$. $N = 256$. $L = 50$ symbols.

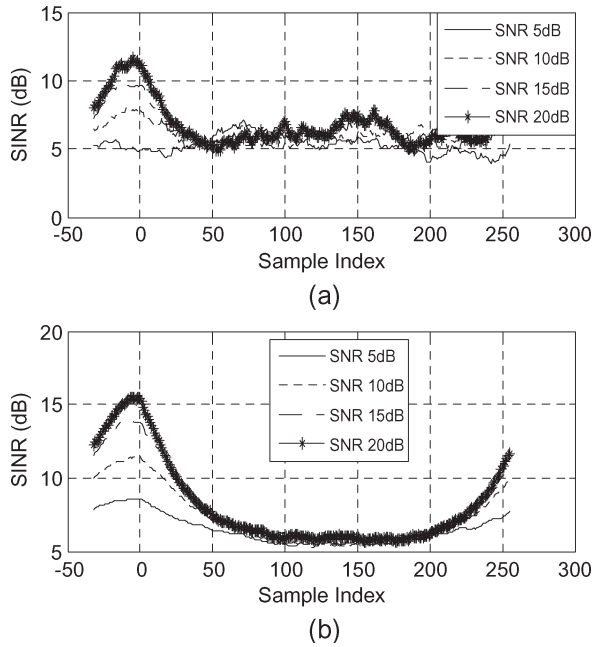

Fig. 4. SINR estimations (14) and (17) against the STO in a time-variant channel are shown in (a) and (b), respectively. NDF $= 0.035$. CFO $= 0$. $N = 256$. $L = 50$ symbols.

In summary, the frequency-oriented estimation is more suitable for the synchronization algorithm than the time-oriented estimation in terms of the estimated SINR profile (i.e., the mentioned first good property of an estimator).

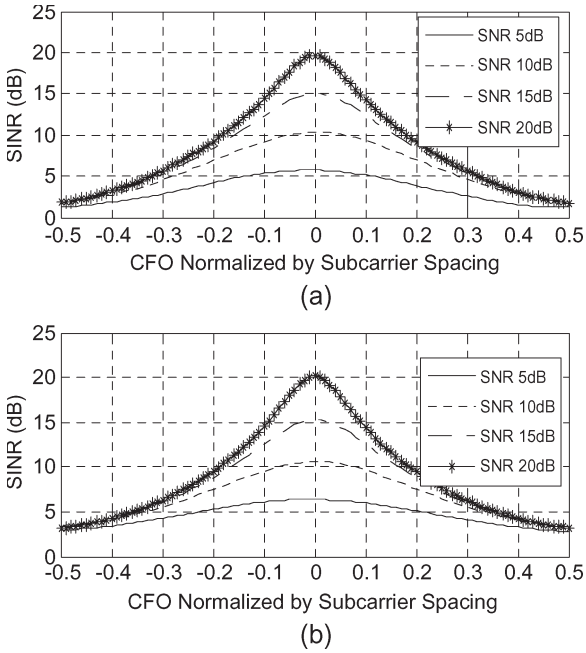

Fig. 5. SINR estimations (14) and (17) against the CFO in a time-invariant channel are shown in (a) and (b), respectively. STO $= 0$. $N = 256$. $L = 50$ symbols.

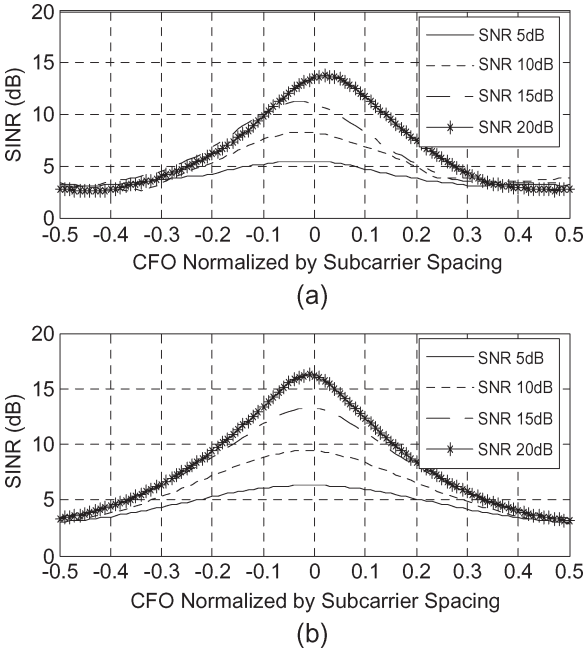

Fig. 6. SINR estimations of (14) and (17) against various CFOs, under the time-variant channel, are shown in (a) and (b), respectively. STO $= 0$. $N = 256$. $L = 50$ symbols.

B. MSINR Synchronization Algorithm

1) MSINR Global Search Algorithm (MSINR-GSA): As we have observed and concluded, the SINR drastically drops due to the incurred interferences from ICI and ISI. Hence, one can intuitively estimate the STO and CFO by maximizing (17) as

$$(\widehat{n}_{\Delta,\mathrm{GSA}}(l), \widehat{\varepsilon}_{f,\mathrm{GSA}}(l)) = \arg\max_{n_\Delta, \varepsilon_f} \{\widehat{\eta}'_l(n_\Delta, \varepsilon_f)\} \quad (18)$$

where $\widehat{n}_{\Delta,\mathrm{GSA}}(l)$ and $\widehat{\varepsilon}_{f,\mathrm{GSA}}(l)$ are the lth symbol's STO and CFO estimates of the 2-D MSINR-GSA, respectively. This is a complicated 2-D search problem. The SINR profile is a unimodal function of the STO and CFO; therefore, without losing too much performance, we separate it into two 1-D processes, i.e., the STO search and the CFO search, as follows:

$$\begin{cases} \widehat{n}'_{\Delta,\mathrm{GSA}}(l) = \arg\max\limits_{n_\Delta} \{\widehat{\eta}'_l(n_\Delta, \widehat{\varepsilon}'_{f,\mathrm{GSA}}(l-1))\} \\ \widehat{\varepsilon}'_{f,\mathrm{GSA}}(l) = \arg\max\limits_{\varepsilon_f} \{\widehat{\eta}'_l(\widehat{n}'_{\Delta,\mathrm{GSA}}(l-1), \varepsilon_f)\} \end{cases} \quad (19)$$

where $\widehat{n}'_{\Delta,\mathrm{GSA}}$ and $\widehat{\varepsilon}'_{f,\mathrm{GSA}}$ are the lth symbol's STO and CFO estimates of the 1-D MSINR-GSA, respectively.

2) MSINR-ELG-ST Recovery Loop: The computational complexity of (19) is still high, because the frequency-domain data and their SINRs have to be obtained over all possible synchronization points. To reduce the computational complexity, instead of searching the whole range of n_Δ, it is assumed that the signal is sampled early at $\widehat{n}_{\Delta,\mathrm{ELG}}(l) - \tau_\Delta$ and late at $\widehat{n}_{\Delta,\mathrm{ELG}}(l) + \tau_\Delta$, where $\widehat{n}_{\Delta,\mathrm{ELG}}(l)$ is the estimated STO of the MSINR-ELG-ST, and τ_Δ is the time shift relative to the estimated symbol boundary. The estimates (17) at these two symbol boundaries are subtracted and filtered to form an error signal $e_\Delta(l)$ [16], [17]. If the samples are, indeed, taken at the left and right samples with the same distance relative to the ideal ST, the error signal is zero for flat-fading channels. For frequency-selective channels, the SINRs at these two samples are generally not the same; however, they are the same under the assumption that the mean of the channel power $E\{|H_k|^2\}$ is the same at all subcarriers. Therefore, the estimated symbol boundary is taken at the midpoint between the two samples. Otherwise, the nonzero error signal is produced to fine-tune the symbol boundary and iteratively make the error signal become zero. The S-curve of the timing discriminator is given by

$$\begin{aligned} e_\Delta(l+1) = {} & \widehat{\eta}'_{l+1}(\widehat{n}_{\Delta,\mathrm{ELG}}(l) - \tau_\Delta, \widehat{\varepsilon}_{f,\mathrm{ELG}}(l)) \\ & - \widehat{\eta}'_{l+1}(\widehat{n}_{\Delta,\mathrm{ELG}}(l) + \tau_\Delta, \widehat{\varepsilon}_{f,\mathrm{ELG}}(l)) \end{aligned} \quad (20)$$

where $\widehat{\varepsilon}_{f,\mathrm{ELG}}(l)$ is the estimated CFO of the lth symbol.

The MSINR ST synchronizer implemented by the ELG is shown in Fig. 7(a). An approximated linear model of the ELG timing recovery loop is shown in Fig. 8, where

$F(z)$	loop filter [22];
K_F	gain of the loop filter;
K_I	intrinsic gain of the timing detector;
K_V	gain of the voltage-controlled oscillator;
$N_\Delta(z)$	z-transform of n_Δ;
$\widehat{N}_\Delta(z)$	z-transform of $\widehat{n}_{\Delta,\mathrm{ELG}}(l)$;
$E_\Delta(z)$	z-transform of $e_\Delta(l)$;
$E'_\Delta(z)$	z-transform of the filtered error signal $e'_\Delta(l)$.

The ST is iteratively adjusted by the VCO as follows:

$$\widehat{n}_{\Delta,\mathrm{ELG}}(l) = \widehat{n}_{\Delta,\mathrm{ELG}}(l-1) + K_V N_S T_S e'_\Delta(l). \quad (21)$$

The closed-loop system equation $L(z) \triangleq \widehat{N}_\Delta(z)/N_\Delta(z)$ can be shown as

$$L(z) = \frac{K_T z^{-1}(1 - a z^{-1})}{1 + z^{-1}(K_T - 2) + z^{-2}(1 - K_T a)} \quad (22)$$

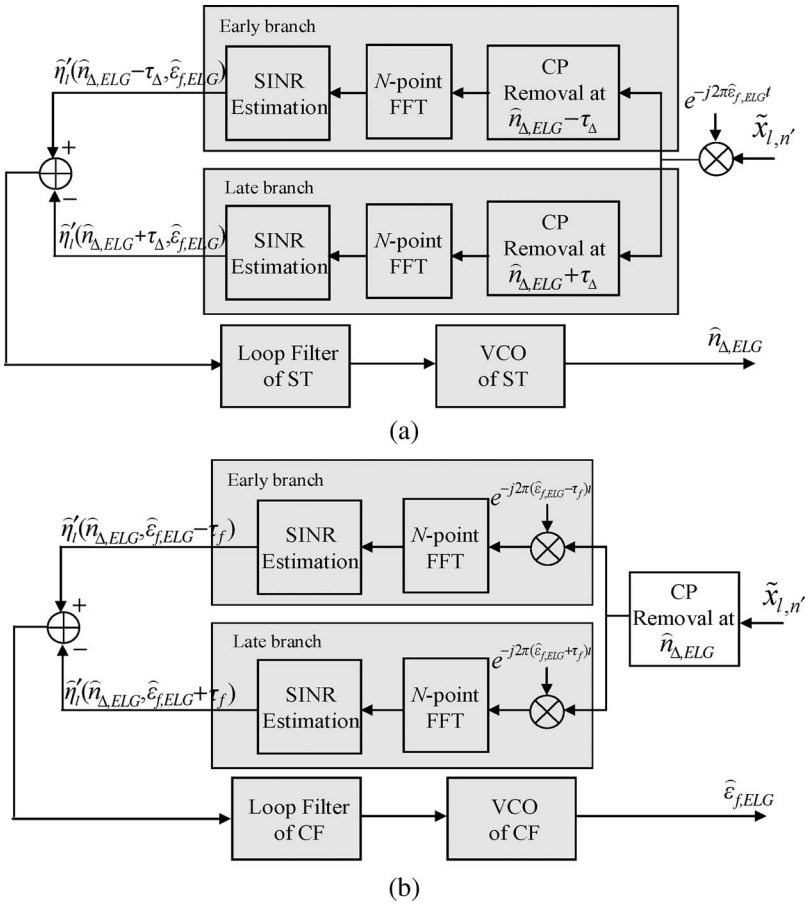

Fig. 7. Architecture of the MSINR-ELG recovery loop. (a) ST synchronizer. (b) CF synchronizer. Note that the symbol indices l in $\widehat{n}_{\Delta,\mathrm{ELG}}(l)$ and $\widehat{\varepsilon}_{f,\mathrm{ELG}}(l)$ are dropped in this figure for notational simplicity.

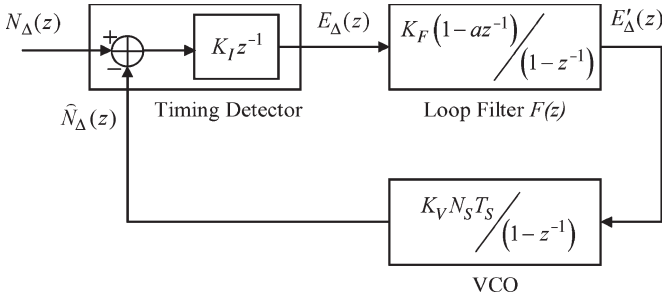

Fig. 8. Approximated discrete-time model of the ELG recovery loop of the ST synchronizer.

where $K_T \triangleq K_F K_I K_V N_S T_S$ is the overall loop gain. The loop is stable under the conditions of

$$0 < a < 1 \quad \text{and} \quad 0 < K_T < \frac{4}{1+a}. \tag{23}$$

With (22), it can be shown that $\lim_{z\to 1} L(z) = 1$. From the final value theorem, this implies that the estimated ST converges toward the ideal ST.

3) MSINR-ELG-CF Recovery Loop: The MSINR CF synchronizer is shown in Fig. 7(b) and is similar to the ST synchronizer, except that the signal is assumed to be shifted in frequency early by $\widehat{\varepsilon}_{f,\mathrm{ELG}}(l) - \tau_f$ and late by $\widehat{\varepsilon}_{f,\mathrm{ELG}}(l) + \tau_f$, where τ_f is the frequency shift relative to the estimated CFO. The S-curve of the frequency discriminator is given by

$$e_f(l+1) = \widehat{\eta}'_l(\widehat{n}_{\Delta,\mathrm{ELG}}(l), \widehat{\varepsilon}_{f,\mathrm{ELG}}(l) - \tau_f) - \widehat{\eta}'_l(\widehat{n}_{\Delta,\mathrm{ELG}}(l), \widehat{\varepsilon}_{f,\mathrm{ELG}}(l) + \tau_f). \tag{24}$$

The CF synchronizer utilizes a similar ELG recovery loop as the ST synchronizer; thus, it is omitted in this paper.

C. ELG Loop Analysis and Design

With (8), by excluding the AWGN, a typical plot of the S-curve (20) (of the timing discriminator) under various CFOs is shown in Fig. 9, which shows that a larger CFO results in a smaller S-curve slope than a smaller CFO, so it is a K_T value. This phenomenon reveals the degradation of the error-tracking performance. The S-curve of the CF synchronizer can similarly be shown and omitted here.

Before introducing the loop design, it must be emphasized that there is no unique optimum design that can be applied to all conditions to the well-known compromise problem between the loop jitter and acquisition time [23], [24]. The overall loop gain is affected by many factors, including all factors that influence the SINR such as synchronization errors and impairments suffered from the channels. In addition, the time shift τ_Δ of the ELG loop affects the intrinsic gain of the timing detector and

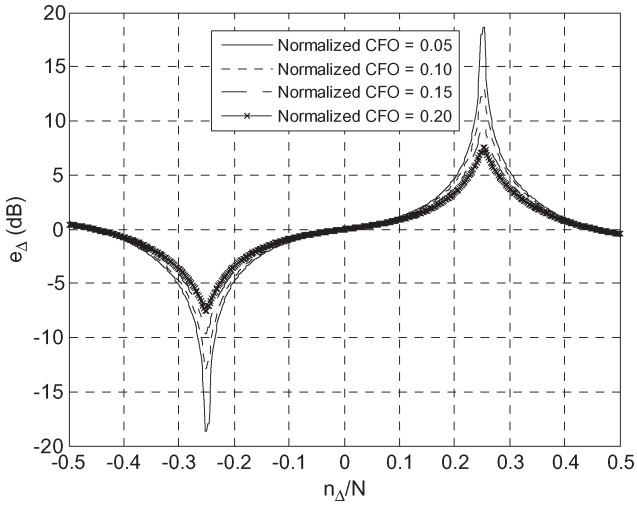

Fig. 9. Theoretical S-curve e_Δ of the ST synchronizer under various CFOs. $\tau_\Delta = N/4$.

the overall loop gain. Before determining the overall loop gain, the intrinsic gain K_I has to be determined first.

By designing for the case of SNR $= 20$ dB and considering the acquisition range, we set the τ_Δ value to 0.25. The intrinsic gain K_I is determined as 32 to best fit the S-curve. The remaining parameters of the ELG loop are configured as follows: $K_F = 1$, $a = 0.9997$, and $K_V N_S T_S = 2 \times 10^{-3}$. Finally, K_T and the normalized loop bandwidth $BN_S T_S$ can be shown to be 0.064 and 0.02, respectively, where B is the loop bandwidth. Therefore, the rise time of the loop is roughly around 50 symbols.

D. Computational Complexity

The computational complexity is dominated by the four FFTs in Fig. 7. An N-point radix-2 FFT roughly requires $(N/2)\log_2 N$ complex multiplications. The squared magnitude of a complex number only costs two real multiplications and one addition, so a squared magnitude operation is roughly counted as a 0.5 complex multiplication. Therefore, the estimation (17) requires $2N$ complex multiplications and N absolute operations. The total amount of complexity is $N((1/2)\log_2 N + 2)$ complex multiplications and N absolute operations for each (early/late) branch. Moreover, one division and one square-root operations are also required in (17) and (16), respectively, which are much less than the FFT operation. The computational complexities of the blind frequency-domain synchronization algorithms [15] and [16] in terms of complex multiplication are roughly $N((1/2)\log_2 N + 1.5)$ and $N((1/2)\log_2 N + 0.75)$, respectively. As shown in this paper, the computational complexity is similar to those in [15] and [16], because the complexity is dominated by the FFT operation, which is the same for all the compared frequency-domain algorithms.

IV. Performance Analysis

A. CRB of the SINR Estimation

To assess the performance of the SINR estimation, the Cramér–Rao lower bound is used as reference. The Cramér–Rao Bound (CRB) of the SINR estimation, for a complex-valued signal embedded in the Gaussian noise, has been derived in [25]. The SINR estimation variance $\sigma\widehat{\eta}^2$ is lower bounded by the CRB and is rewritten as

$$\frac{\sigma^2_{\widehat{\eta}}}{\eta^2} \geq 2\left(\frac{2}{N\eta} + \frac{1}{N}\right) \tag{25}$$

where η is the true SINR. The CRB of the SINR estimation is used to assess the performance of the synchronizers in the following section.

B. Performance Analysis of the MSINR-ELG Synchronizers

The lower bound of the mean-squared error (MSE) for the ST tracking loop is derived as follows. As depicted in Fig. 9, in the vicinity of the ideal synchronization point, the S-curve is roughly linear and can be approximated as

$$e_\Delta \approx K_I' n_\Delta \tag{26}$$

where K_I' is the slope of the S-curve at the ideal synchronization point. With (20) and (26), assuming that the SINR variances are equivalent for both the early and late branches in the vicinity of the ideal synchronization point, the ST variance $\sigma^2_{n_\Delta}$ can be determined as

$$\sigma^2_{n_\Delta} = \frac{2\sigma^2_{\widehat{\eta}}}{K_I'^2}. \tag{27}$$

Note that the factor in (27) is 2 because there are two subtraction terms in the RHS of (20). Furthermore, if we assume that the ST estimation error is a wide-sense stationary white-noise process, after being filtered by $L(z)$, as depicted in Fig. 8, the MSE of the synchronizer can be written as

$$\begin{aligned} E\left[\left(\widehat{n}_{\Delta,\mathrm{ELG}}(l) - n_\Delta\right)^2\right] &\geq \sigma^2_{\widehat{n}_\Delta} \\ &= \frac{\sigma^2_{\widehat{n}_\Delta}}{2\pi j}\oint_C L(z)L(z^{-1})z^{-1}dz \end{aligned} \tag{28}$$

where $j = \sqrt{-1}$. By inserting (27) into (28), we have

$$E\left[\left(\widehat{n}_{\Delta,\mathrm{ELG}}(l) - n_\Delta\right)^2\right] \geq \frac{2}{K_I'^2}\frac{\sigma^2_{\widehat{n}_\Delta}}{2\pi j}\oint_C L(z)L(z^{-1})z^{-1}dz. \tag{29}$$

Next, the contour integral in (29) can explicitly be solved. With (22) and the parameters in Section III-C, the partial fraction expansion of $L(z)$ can be shown as

$$L(z) = \frac{-1.43309 \times 10^{-6}}{z - 9.99699 \times 10^{-1}} + \frac{6.40014 \times 10^{-2}}{z - 9.36301 \times 10^{-1}}. \tag{30}$$

Consequently, the contour integral in (29) can be solved using the Cauchy integral theorem, and (29) can be reduced to

$$E\left[\left(\widehat{n}_{\Delta,\mathrm{ELG}}(l) - n_\Delta\right)^2\right] \geq 3.32077 \times 10^{-2} \times \frac{2\sigma^2_{\widehat{\eta}}}{K_I'^2}. \tag{31}$$

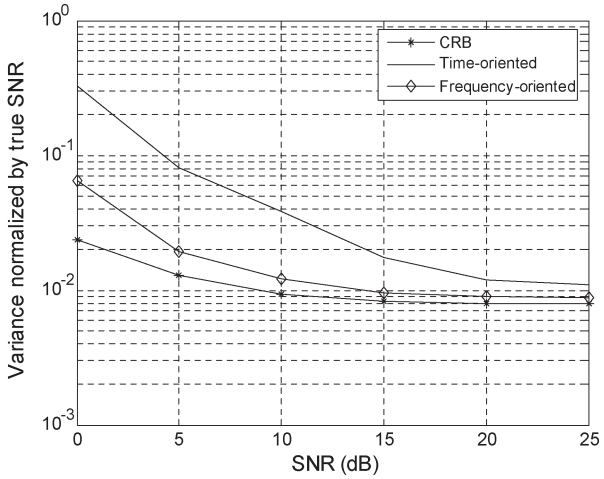

Fig. 10. SINR estimation variances against the SNR. NDF $= 0.035$.

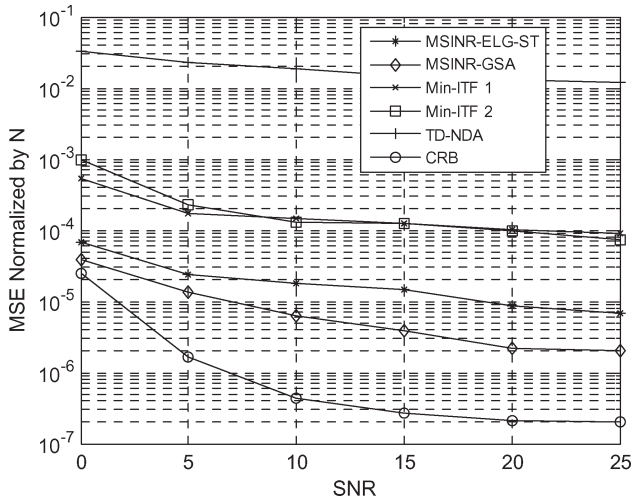

Fig. 11. MSEs of the compared ST synchronizers against the SNR. NDF $= 0.0$. CFO $= 0.1$.

Finally, by inserting (25) into (31), the MSE lower bound of the tracking loop can be determined as

$$E\left[\left(\widehat{n}_{\Delta,\mathrm{ELG}}(l)-n_{\Delta}\right)^2\right] \geq 1.32831\times 10^{-1}\times\frac{\eta(2+\eta)}{K_I'^2 N}. \quad (32)$$

Clearly, the bound depends on the SINR, the characteristic of the S-curve, and the closed-loop system equation. The MSE lower bound of the CF synchronizer uses the same inequality as (28), except that the characteristic of the S-curve and the closed-loop system equation are replaced with those used in the CF synchronizer.

V. Simulations

A. Comparison of the Proposed SINR Estimations

The frequency-oriented (17) and the time-oriented (14) estimations have qualitatively been compared by the estimated SINR profiles in Section III-A3. In this section, these two different estimations will quantitatively be evaluated by comparing their variances based on the same system in Section III-A3. The estimation variances against the SNR are plotted in Fig. 10. The CRB (25) is also shown. As it can be seen, the frequency-oriented estimation has a smaller variance and is closer to the CRB than the time-oriented estimation.

In summary, the frequency-oriented estimation is more suitable for synchronization error estimations than the time-oriented estimation in terms of the estimation's variance (i.e., the mentioned second good property of an estimator in Section III-A).

B. Performance of the Proposed Synchronizer

We use Monte Carlo simulations to evaluate the performance of the synchronizers and consider an OFDM system of $N = 256$ subcarriers and a guard interval of $N_G = N/8 = 32$ samples. Only data subcarriers are assumed. The simulated modulation scheme is quadrature phase-shift keying. The signal bandwidth is assumed to be 2.5 MHz, and the radio frequency is 2.4 GHz. The subcarrier spacing is 8.68 kHz. The OFDM symbol duration is 115.2 μs. The CFO is 10% of the subcarrier spacing, i.e., 0.87 kHz, in all simulations. To verify the performance of the proposed technique, the channel is assumed to have N_G paths. Therefore, the Good-ST region contains only one sample. The channel taps h_τ are randomly generated by independent zero-mean unit-variance complex Gaussian variables with $\sum_\tau E\{|h_\tau|^2\} = 1$ for each simulation run, where τ is the path delay. In each simulation run, 10 000 OFDM symbols are tested. We evaluate the performances of the synchronizers by using the estimations' normalized MSE. All the results are obtained by averaging more than 2000 independent channel realizations.

1) ST Estimation Performance: For the ST estimation, we compare the proposed technique with the following blind or NDA techniques by assuming the same system settings: 1) blind minimum-interference ST estimator (Min-ITF 1) [16], 2) blind minimum-interference ST estimator (Min-ITF 2) [15], and 3) NDA ML ST estimator (TD-NDA) [5]. The ST estimator in [17] is data aided, so it is not considered here.

The MSEs of the estimated ST against the SNR in time-invariant and time-variant channels are shown in Figs. 11 and 12, respectively. The NDF $= 0.035$ corresponds to a maximum Doppler frequency of 303.8 Hz, i.e., a mobile speed of 117 km/hr. In addition to the MSEs of the MSINR-ELG-ST and MSINR-GSA (18), the CRB (29) is also shown in Fig. 11. Note that K_I' is obtained by simulation. As it can be seen, the MSINR synchronizer achieves a smaller MSE than the compared synchronizers. The performance of the TD-NDA is not as good as the compared techniques, because the correlation result of the CP is vulnerable to the incurred ISI. In addition, the performance of the MSINR-GSA is better than the MSINR-ELG-ST. However, their performances are not too far apart. Therefore, the complexity can greatly be reduced by the ELG technique while not losing too much performance.

The estimated STs of the MSINR-ELG-ST against symbol index under various SNRs in time-invariant and time-variant channels are shown in Figs. 13 and 14, respectively. As shown in these figures, the estimated ST is around the Good-ST region (at the zeroth sample). However, the estimated ST gradually drifts away from the Good-ST region when the SNR decreases.

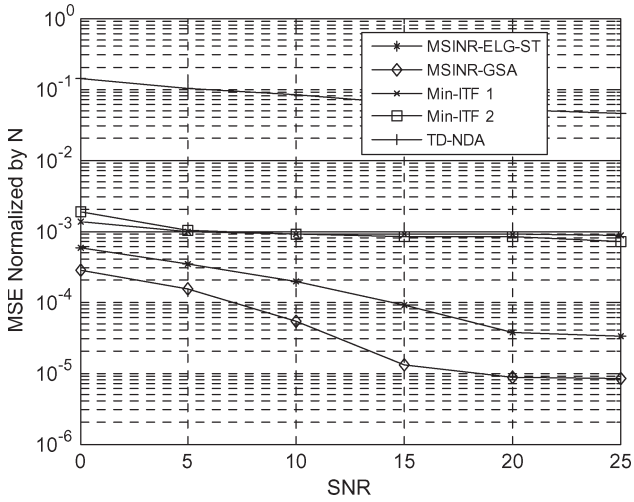

Fig. 12. MSEs of the compared ST synchronizers against the SNR. NDF $= 0.035$. CFO $= 0.1$.

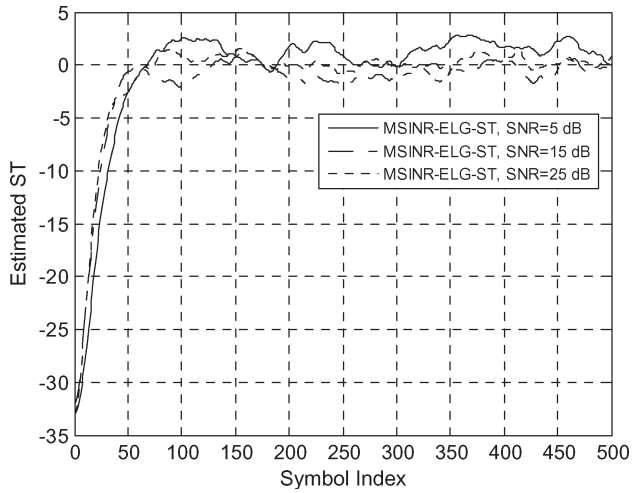

Fig. 13. Acquisition time of the MSINR ST synchronizer under various SNRs. NDF $= 0.0$. CFO $= 0.1$.

2) CFO Estimation Performance: For the CFO estimation, we compare the proposed technique with the TD-NDA CFO estimation in [5]. The MSEs of the estimated CFO against the SNR in time-invariant and time-variant channels are shown in Figs. 15 and 16, respectively. In addition to the MSEs of the MSINR-ELG-CF and MSINR-GSA (18), the CRB is also shown in Fig. 15, where the MSINR synchronizer achieves a smaller MSE than the compared synchronizer. In addition, the ELG technique greatly reduces the complexity of the MSINR-GSA with a close performance to it.

The estimated CFOs of the MSINR-ELG-CF against symbol index under various SNRs in time-invariant and time-variant channels are shown in Figs. 17 and 18, respectively, where the estimated CFO is around the true CFO $= 0.87$ kHz. When the SNR decreases, the acquisition time apparently increases. The acquisition time is affected by the closed-loop bandwidth of the ELG recovery loop. When the SNR decreases, the closed-loop gain and bandwidth accordingly decrease. This slows down the acquisition time.

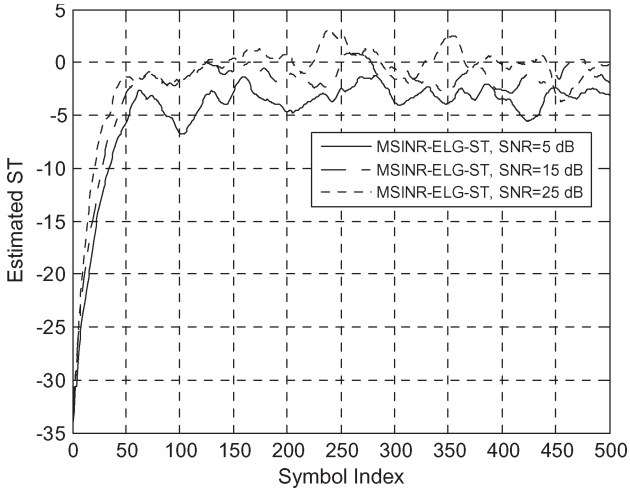

Fig. 14. Acquisition time of the MSINR ST synchronizer under various SNRs. NDF $= 0.035$. CFO $= 0.1$.

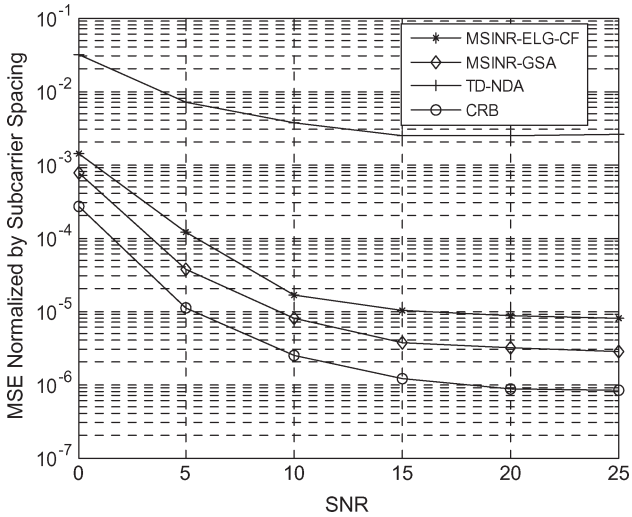

Fig. 15. MSEs of the compared CF synchronizers against the SNR. NDF $= 0.0$. CFO $= 0.1$.

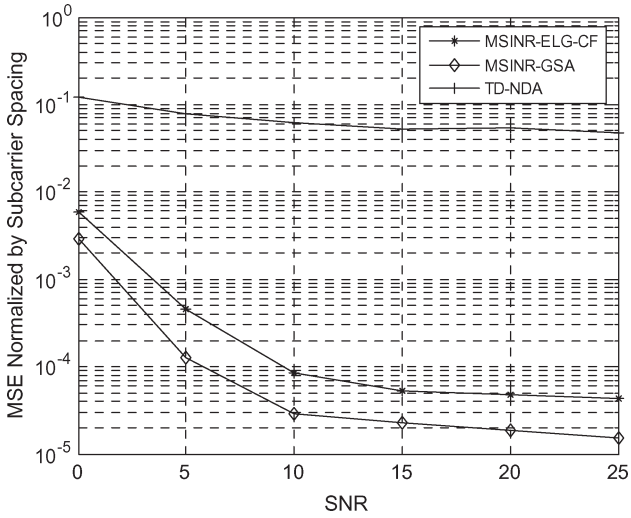

Fig. 16. MSEs of the compared CF synchronizers against the SNR. NDF $= 0.035$. CFO $= 0.1$.

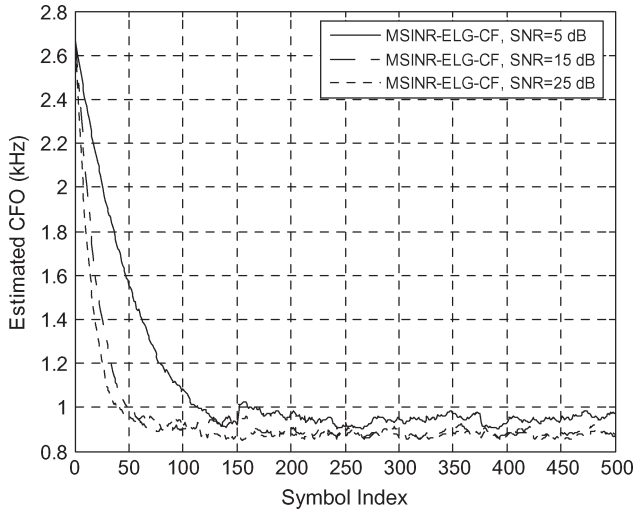

Fig. 17. Acquisition time of the MSINR CF synchronizer under various SNRs. NDF $= 0.0$. CFO $= 0.1$.

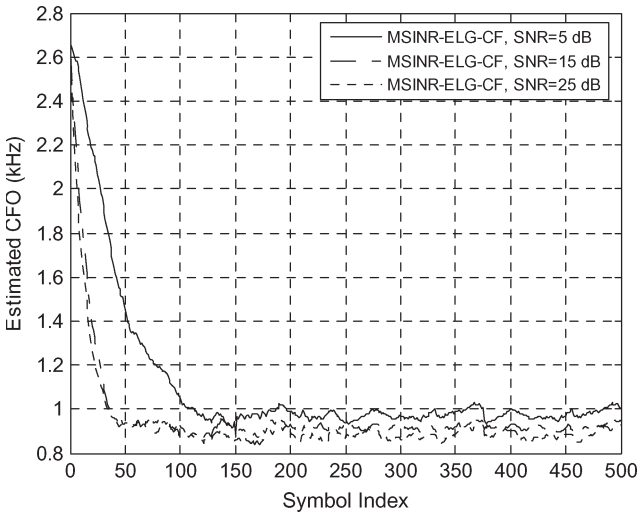

Fig. 18. Acquisition time of the MSINR CF synchronizer under various SNRs. NDF $= 0.035$. CFO $= 0.1$.

VI. Conclusion

In the literature, the synchronization problem has been treated by the viewpoint of the estimation theory, for example, the ML approach. In this paper, we have intuitively dealt with this problem by maximizing the SINR. The proposed technique is NDA and independent of the signal structure. For the MSINR synchronization algorithm, two blind SINR estimations have been investigated. The frequency-oriented SINR estimation has been found to be more suitable for the MSINR algorithm than the time-oriented SINR estimation. Moreover, it has been shown that the proposed ELG tracking loop is a good compromise between the performance and complexity.

Acknowledgment

The authors would like to thank the Editor and the anonymous Reviewers for their helpful comments and suggestions, which have improved the quality of this paper.

References

[1] J. A. C. Bingham, "Multicarrier modulation for data transmission: An idea whose time has come," *IEEE Commun. Mag.*, vol. 28, no. 5, pp. 5–14, May 1990.
[2] B. Lefloch, M. Alard, and C. Berrou, "Coded orthogonal frequency-division multiplex," *Proc. IEEE*, vol. 83, no. 6, pp. 982–996, Jun. 1995.
[3] M. Rohling, T. May, K. Bruninghaus, and R. Grunheid, "Broadband OFDM radio transmission for multimedia applications," *Proc. IEEE*, vol. 87, no. 10, pp. 1778–1789, Oct. 1999.
[4] J. Chuang and N. Sollenberger, "Beyond 3G: Wideband wireless data access based on OFDM and dynamic packet assignment," *IEEE Commun. Mag*, vol. 38, no. 7, pp. 78–87, Jul. 2000.
[5] J. J. van de Beek, M. Sandell, and P. O. Börjesson, "ML estimation of time and frequency offset in OFDM systems," *IEEE Trans. Signal Process.*, vol. 45, no. 7, pp. 1800–1805, Jul. 1997.
[6] H. Minn, V. K. Bhargava, and K. B. Letaief, "A robust timing and frequency synchronization for OFDM systems," *IEEE Trans. Wireless Commun.*, vol. 2, no. 4, pp. 822–839, Jul. 2003.
[7] M. Speth, S. Fechtel, G. Fock, and H. Meyr, "Optimum receiver design for OFDM-based broadband transmission—Part II: A case study," *IEEE Trans. Commun.*, vol. 49, no. 4, pp. 571–578, Apr. 2001.
[8] Y. H. Kim, I. Song, S. Yoon, and S. R. Park, "An efficient frequency offset estimator for OFDM systems and its performance characteristics," *IEEE Trans. Veh. Technol.*, vol. 50, no. 5, pp. 1307–1312, Sep. 2001.
[9] T. M. Schmidl and D. C. Cox, "Robust frequency and timing synchronization for OFDM," *IEEE Trans. Commun.*, vol. 45, no. 12, pp. 1613–1621, Dec. 1997.
[10] B. Park, H. Cheon, C. Kang, and D. Hong, "A novel timing estimation method for OFDM systems," *IEEE Commun. Lett.*, vol. 7, no. 5, pp. 239–241, May 2003.
[11] K. Shi and E. Serpedin, "Coarse frame and carrier synchronization of OFDM systems: A new metric and comparison," *IEEE Trans. Wireless Commun.*, vol. 3, no. 4, pp. 1271–1284, Jul. 2004.
[12] M. H. Cheng and C. C. Chou, "Maximum-likelihood estimation of frequency and time offsets in OFDM systems with multiple sets of identical data," *IEEE Trans. Signal Process.*, vol. 54, no. 7, pp. 2848–2852, Jul. 2006.
[13] K. Ramasubramanian and K. Baum, "An OFDM timing recovery scheme with inherent delay-spread estimation," in *Proc. IEEE GLOBECOM*, Nov. 2001, vol. 5, pp. 3111–3115.
[14] D. Lee and K. Cheun, "Coarse symbol synchronization algorithms for OFDM systems in multipath channels," *IEEE Commun. Lett.*, vol. 6, no. 10, pp. 446–448, Oct. 2002.
[15] Q. Zhu and Z. Liu, "Minimum interference blind time-offset estimation for OFDM systems," *IEEE Trans. Wireless Commun.*, vol. 5, no. 8, pp. 2136–2142, Aug. 2006.
[16] A. J. Al-Dweik, "A novel non-data-aided symbol timing recovery technique for OFDM systems," *IEEE Trans. Commun.*, vol. 54, no. 1, pp. 37–40, Jan. 2006.
[17] G. Santella, "A frequency and symbol synchronization system for OFDM signals: Architecture and simulation results," *IEEE Trans. Veh. Technol.*, vol. 49, no. 1, pp. 254–275, Jan. 2000.
[18] M. Speth, S. Fechtel, G. Fock, and H. Meyr, "Optimum receiver design for wireless broad-band systems using OFDM—Part I," *IEEE Trans. Commun.*, vol. 47, no. 11, pp. 1668–1677, Nov. 1999.
[19] J. Li and M. Kavehrad, "Effects of time selective multipath fading on OFDM systems for broadband mobile applications," *IEEE Commun. Lett.*, vol. 3, no. 12, pp. 332–334, Dec. 1999.
[20] Y. Mostofi and D. C. Cox, "Mathematical analysis of the impact of timing synchronization errors on the performance of an OFDM system," *IEEE Trans. Commun.*, vol. 54, no. 2, pp. 226–230, Feb. 2006.
[21] T. R. Benedict and T. T. Soong, "The joint estimation of signal and noise from the sum envelope," *IEEE Trans. Inf. Theory*, vol. IT-13, no. 3, pp. 447–454, Jul. 1967.
[22] H. Meyr, M. Moeneclaey, and S. A. Fechtel, *Digital Communication Receivers, Synchronization, Channel Estimation and Signal Processing*. Hoboken, NJ: Wiley, 1998.
[23] A. Al-Dweik and R. El-Khazali, "A modified early–late gate for blind symbol timing recovery of OFDM systems," *IEICE Trans. Commun.*, vol. E89-B, no. 1, pp. 11–18, Jan. 2006.
[24] F. Gardner, *Phaselock Techniques*. New York: Wiley, 1979.
[25] D. R. Pauluzzi and N. C. Beaulieu, "A comparison of SNR estimation techniques for the AWGN channel," *IEEE Trans. Commun.*, vol. 48, no. 10, pp. 1681–1691, Oct. 2000.

Wen-Long Chin received the B.S. degree in electronics engineering from National Chiao Tung University, Hsinchu, Taiwan, in 1994, the M.S. degree in electrical engineering from the National Taiwan University, Taipei, Taiwan, in 1996, and the Ph.D. degree in electronics engineering from National Chiao Tung University, Hsinchu, in 2008.

In February 2009, he joined National Cheng Kung University, Tainan, Taiwan, as an Assistant Professor. His research interests lie in the areas of (VLSI) signal processing, communications, and networks. Before holding the faculty position, he had been with the Hsinchu Science Park for over 11 years, where he was in charge of communications and IC designs.

Sau-Gee Chen received the B.S. degree from the National Tsing Hua University, Hsinchu, Taiwan, in 1978 and the M.S. and Ph.D. degrees in electrical engineering from the State University of New York, Buffalo, in 1984 and 1988, respectively.

From 2003 to 2006, he was the Director of the Institute of Electronics, Department of Electronics Engineering, National Chiao Tung University, Hsinchu, where he is currently a Professor. His research interests include digital communication, multimedia computing, digital signal processing, and VLSI signal processing. He has published more than 70 conference proceedings and journal papers and is the holder of several U.S. and Taiwan patents.